ACS Photonics

Article

pubs.acs.org/journal/apchd5

Ligand-Free, Colloidal, and Plasmonic Silicon Nanocrystals Heavily Doped with Boron

Shu Zhou,[†,‡] Zhenyi Ni,[†] Yi Ding,[§] Michihiro Sugaya,[‡] Xiaodong Pi,[*,†] and Tomohiro Nozaki[*,‡]

[†]State Key Laboratory of Silicon Materials & School of Materials Science and Engineering, Zhejiang University, Hangzhou, 310027, China

[‡]Department of Mechanical Science and Engineering, Tokyo Institute of Technology, Meguro, Tokyo 152-8550, Japan

[§]Institute of Photoelectronic Thin Film Devices and Technology, Tianjin Key Laboratory of Photoelectronic Thin Film Devices and Technology, Nankai University, Tianjin 300071, China

S *Supporting Information*

ABSTRACT: Colloidal heavily doped silicon nanocrystals (Si NCs) exhibiting tunable localized surface plasmon resonance (LSPR) are of great interest in cost-effective, solution-processed optoelectronic devices given the abundance and nontoxicity of Si. In this work we show that tunable plasmonic properties and colloidal stability without the use of ligands can be simultaneously obtained for Si NCs heavily doped with boron (B). The heavily B-doped Si NC colloids are found to be stable in air for months, opening up the possibility of device processing in ambient atmosphere. The optical absorption of heavily B-doped Si NCs reveals that the heavy B doping not only changes the concentration of free carriers that are confined in Si NCs but also modifies the band structure of Si NCs. After heavy B doping both indirect and direct electronic transition energies remarkably decrease in Si NCs because the heavy B doping induced movement of the conduction band toward the band gap could be more significant than that of the Fermi level into the valence band. The LSPR of heavily B-doped Si NCs originates from free holes above the Fermi level, which are largely from the B-induced impurity band.

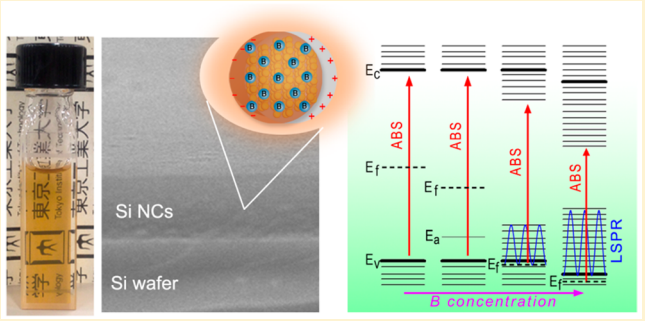

KEYWORDS: *silicon nanocrystals, colloid, localized surface plasmon resonance, band gap, heavy doping*

As an emerging new class of plasmonic nanomaterials, heavily doped semiconductor nanocrystals (NCs) with localized surface plasmon resonance (LSPR) have received great attention in the past few years because of their potential applications in novel optoelectronic devices.[1−3] In contrast to conventional metal NCs, the plasmonic properties of heavily doped semiconductor NCs are largely dependent on the tunable concentration of free carriers that are confined in semiconductor NCs. The tunability of the free carrier concentration of semiconductor NCs may be realized either by intrinsically introducing defects or extrinsically doping impurities.[4−11] Despite recent impressive progress made on the heavy-doping-enabled LSPR of semiconductor NCs, the applications of plasmonic semiconductor NCs in optoelectronic devices remain challenging. Creating stable heavily doped semiconductor-NC colloids is particularly demanded for the integration of the doping-enabled plasmonic properties with high-performance, low-cost optoelectronic devices, given the fact that uniform and dense thin films may be inexpensively fabricated by using printing.[12−15] A common method to obtain stable semiconductor-NC colloids is the functionalization of the surface of semiconductor NCs by using organic ligands, which effectively suppress the van der Waals force induced agglomeration of semiconductor NCs.[16−21] However, it becomes exceedingly difficult to functionalize the surface of heavily doped semiconductor NCs because some of the doped impurities inevitably reside at the NC surface,[22−24] leading to a significant change of the surface chemistry of semiconductor NCs. Moreover, it should be noted that organic ligands at the NC surface may seriously hinder the transport of carriers in semiconductor-NC films,[25−28] even if the surface of heavily doped semiconductor NCs are successfully functionalized with organic ligands.

As one of the most important semiconductor NCs, silicon (Si) NCs may be heavily doped to exhibit mid-infrared LSPR.[8,9,11,29] In contrast, the LSPRs of other NCs are routinely limited in the visible and near-infrared regions.[2−5,7] It is additionally known that Si is abundant and nontoxic. Therefore, heavily doped Si NCs hold considerable promise for plasmonics. Wheeler et al.[30] have recently indicated that the colloidal stability of plasmonic Si NCs can be confronted by functionalizing the NC surface with highly electronegative chlorine (Cl). The large bond polarization induced by Cl induces a hypervalent interaction between the NC surface and

Received: October 4, 2015
Published: February 10, 2016

DOI: 10.1021/acsphotonics.5b00568
ACS Photonics 2016, 3, 415−422

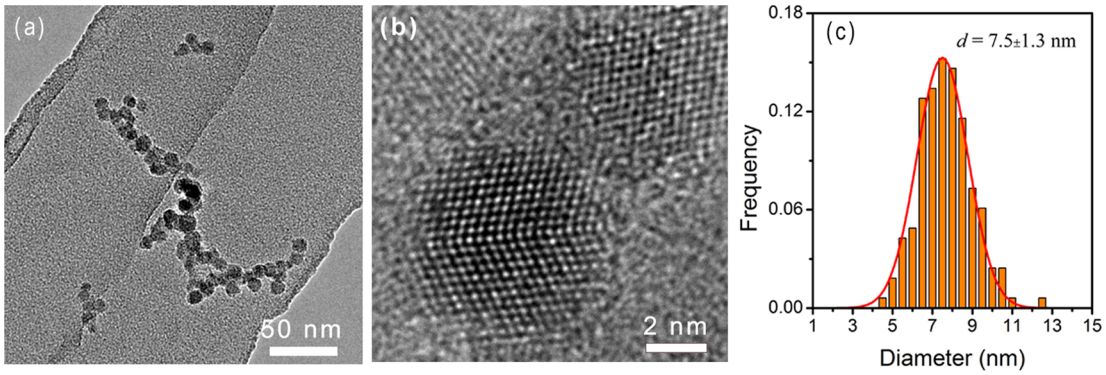

Figure 1. (a) Low-resolution TEM image, (b) high-resolution TEM image, and (c) size distribution of Si NCs heavily doped with B at the concentration of ~7%.

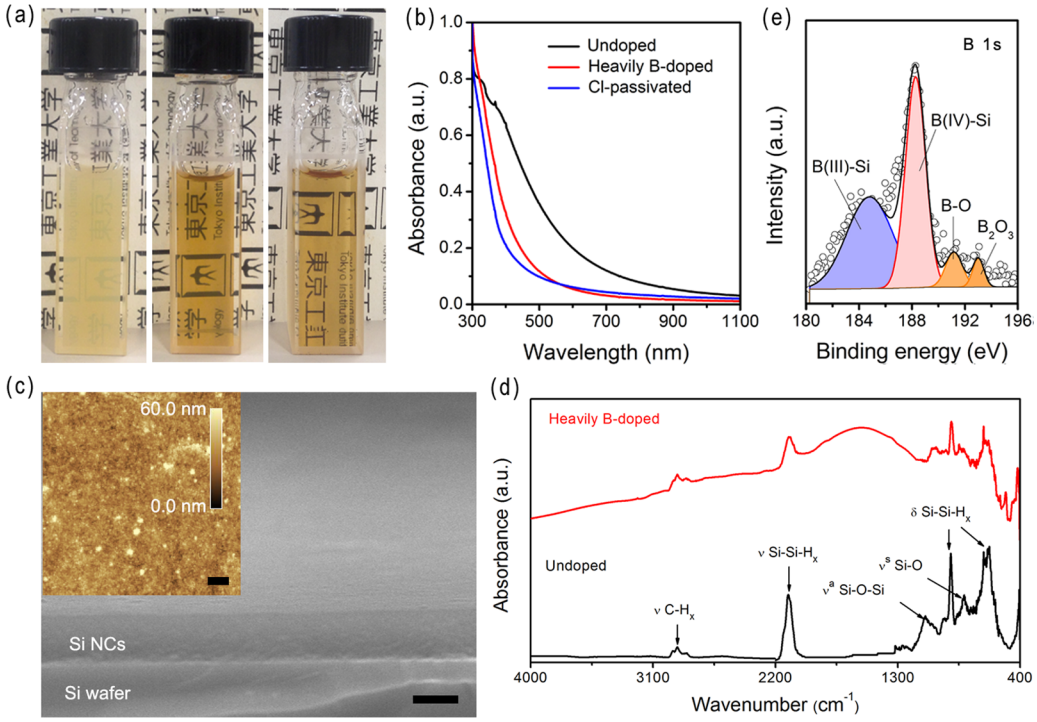

Figure 2. (a) Photographs of undoped Si NCs (left), heavily B-doped Si NCs (middle), and Cl-passivated Si NCs (right) in benzonitrile. The concentrations for all Si NCs in benzonitrile are 0.04 mg/mL. (b) UV−vis absorption spectra of undoped Si NCs, heavily B-doped Si NCs, and Cl-passivated Si NCs in benzonitrile. (c) Scanning electron microscopy (SEM) and atomic force microscopy (AFM) (inset) show that a continuous, dense, and smooth film is obtained by drop-casting heavily B-doped Si NC colloid on a Si substrate. Scale bar, 2 μm. (d) FTIR spectra of undoped and heavily B-doped Si NCs. (e) X-ray photoelectron spectra of heavily B-doped Si NCs. In the B 1s spectrum the peaks at 184.8 (blue) and 188.3 eV (red) originate from the B atoms bonded to three Si atoms (B(III)−Si) and B atoms bonded to four Si atoms (B(IV)−Si), respectively. The two higher energy peaks at 191.2 and 193.0 eV (orange) are due to B atoms bonded with O. The concentration of B for heavily doped Si NCs is ~7%.

hard donor molecules, providing the heavy doping and colloidal stability of Si NCs. But the plasmonic properties of Si NCs are unlikely to be widely tuned by the hypervalent interaction. In addition, Si−Cl bonds are not stable in air,[31−34] limiting the processing of Si NCs inside an inert atmosphere.

In this work, we demonstrate that tunable infrared LSPR and colloidal stability can be realized at the same time for heavily boron (B)-doped Si NCs without the use of ligands. The effect of heavy B doping on the band structure of Si NCs has been explored by optical absorption measurements. It is found that the heavy B doping leads to a decrease of the energy for both the indirect and direct electronic transitions in Si NCs because the heavy B doping induced move of the conduction band toward the band gap could be more significant than that of the Fermi level into the valence band. The knowledge on the band structure of heavily B-doped Si NCs helps clarify the origin of LSPR in heavily doped semiconductor NCs.

RESULTS AND DISCUSSION

Both undoped and heavily B-doped Si NCs have been synthesized by using a SiH_4-based nonthermal plasma.[23,35−37] After storage in air for 15 months both undoped and heavily B-doped Si NCs are treated with hydrofluoric acid (HF) to render a much less defective NC surface.[38] The resulting hydrogen (H)-passivated NCs are characterized by using transmission electron microscopy (TEM). It is found that heavy B doping hardly changes the size and crystallinity of Si NCs (Figure S1 in the Supporting Information). Figure 1

DOI: 10.1021/acsphotonics.5b00568
ACS Photonics 2016, 3, 415−422

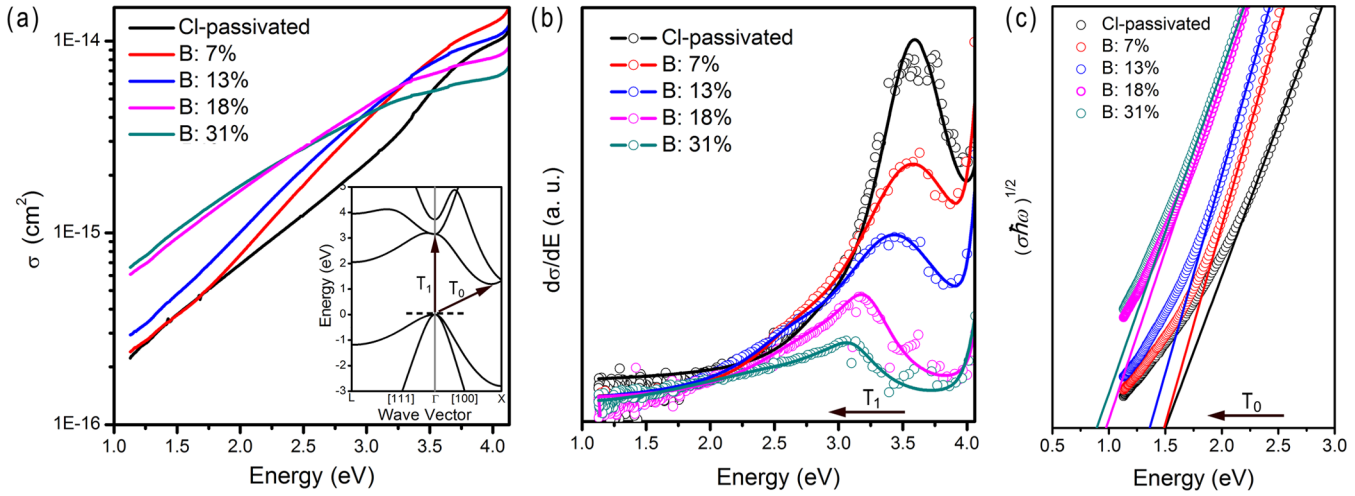

Figure 3. (a) Per-NC absorption spectra of Cl-passivated Si NCs and heavily B-doped Si NCs in benzonitrile. The inset shows the band structure of bulk Si in which the indirect phonon-assisted Γ−X transition (T_0) and direct Γ−Γ transition (T_1) are indicated. (b) Derivative absorption spectra of Cl-passivated Si NCs and heavily B-doped Si NCs in benzonitrile. (c) Absorption data for Cl-passivated Si NCs and heavily B-doped Si NCs in benzonitrile plotted as $(\sigma\hbar\omega)^{1/2}$. The concentrations of B are ∼7%, 13%, 18%, and 31%.

representatively shows the TEM results for Si NCs doped with B at a concentration of ∼7%. The low-resolution TEM image (Figure 1a) and high-resolution TEM image (Figure 1b) clearly show sphere-like Si NCs. In addition to lattice fringes, twining is also observed in the high-resolution TEM image (Figure 1b), characteristic of the heavy B doping of Si NCs.[9] The average size of Si NCs is found to be 7.5 ± 1.3 nm by analyzing their size distributions (Figure 1c).

Colloidal Stability. It is well-known that undoped Si NCs are not soluble in most nonpolar solvents.[39] The choice of appropriate polar solvents such as benzonitrile may enable dilute solutions of undoped Si NCs after sonification,[40] but undoped Si NCs agglomerate quickly. Figure 2a shows the resulting cloudy dispersion of undoped Si NCs (left image). In contrast to undoped Si NCs, heavily B-doped Si NCs may be readily dispersed in benzonitrile, leading to an optically transparent colloid (Figure 2a, middle image). This indicates that the agglomeration of Si NCs in benzonitrile is essentially suppressed by heavy B doping. The dispersibility of heavily B-doped Si NCs in benzonitrile is basically as good as that of Cl-passivated undoped Si NCs (Figure 2a, right image). Figure 2b shows the UV−vis absorption spectra of the benzonitrile solutions of undoped, heavily B-doped, and Cl-passivated Si NCs. Due to the agglomeration-induced light scattering, undoped Si NCs exhibit apparent optical absorption when the wavelength is > ∼600 nm. However, the optical absorbance of heavily B-doped Si NCs and Cl-passivated Si NCs are almost zero in the long-wavelength region because their light scattering is negligible (Figure S2 in the Supporting Information). The stability of heavily B-doped Si NCs in benzonitrile has been studied by recording the optical absorption of the colloids during the course of storage in air (Figure S3 in the Supporting Information). It can be seen that there is almost no change in the absorption spectra as storage time in air increases up to 4 months (Figure S3 in the Supporting Information). Therefore, we claim that heavily B-doped Si NCs are readily well-dispersed and highly stable in benzonitrile. We would like to point out that the Cl-passivated Si NCs strongly agglomerate and precipitate in benzonitrile after they are stored in air for a few days because of the instability of Si−Cl bonds at the NC surface.[31−34] The colloidal stability in air provided by heavy B doping in air opens up the possibility of the processing of devices that are based on Si NC films in ambient atmosphere. Figure 2c shows the scanning electronic microscopy (SEM) image of a continuous and dense film obtained by drop-casting a 5 mg/mL benzonitrile solution of Si NCs heavily doped with B at the concentration of ∼7% onto a Si substrate in air. The film is rather smooth, with an average roughness of 15 nm, which is measured with atomic force microscopy (AFM) (inset of Figure 2c). It is the excellent dispersion of heavily B-doped Si NCs in benzonitrile that enables the continuity and smoothness of the Si NC film.

The colloidal stability of Si NCs in benzonitrile is largely dependent on their surface chemistry.[39,40] We have used Fourier transform infrared (FTIR) spectroscopy to characterize the Si NC films casted from the colloids of undoped and heavily B-doped Si NCs. Figure 2d shows the obtained FTIR results for both undoped and heavily B-doped Si NCs. For undoped Si NCs, the most prominent peaks at ∼640, 890, and 2100 cm^{-1} are basically related to the vibration of Si−H bonds.[41] Small peaks at ∼810 and 1100 cm^{-1} associated with the Si−O stretching mode[41] can also be observed in the spectrum, indicating a little O exists at the NC surface. These peaks are all present in the FTIR spectrum of heavily B-doped Si NCs. No vibration modes related to B−H bonds are found in the FTIR spectrum, indicating that H prefers bonding with a Si atom over a B atom at the NC surface. The existence of B at the surface of heavily B-doped Si NCs is evaluated by using X-ray photoelectron spectroscopy (XPS), as shown in Figure 2e. The B 1s spectrum indicates that there are B atoms at the surface or subsurface of Si NCs. In the B 1s spectrum, the peak at 188.3 eV is related to B atoms that are bonded with four Si atoms (B(IV)−Si),[42] while the peak at 184.8 eV means a B atom is linked with three Si atoms (B(III)−Si).[43] The small peaks at 191.2 and 193.0 eV are associated with oxidized B,[43] indicating very little O at the NC surface. Since H cannot give rise to enough steric force to enable stable dispersion of Si NCs, B at the surface or subsurface of Si NCs should be responsible for the stable heavily B-doped Si NC colloids. It has been previously shown that in B and phosphorus (P) co-doped Si NCs a negative potential occurs at the NC surface because of ionized B atoms at the surface side and ionized P atoms at the

DOI: 10.1021/acsphotonics.5b00568
ACS Photonics 2016, 3, 415−422

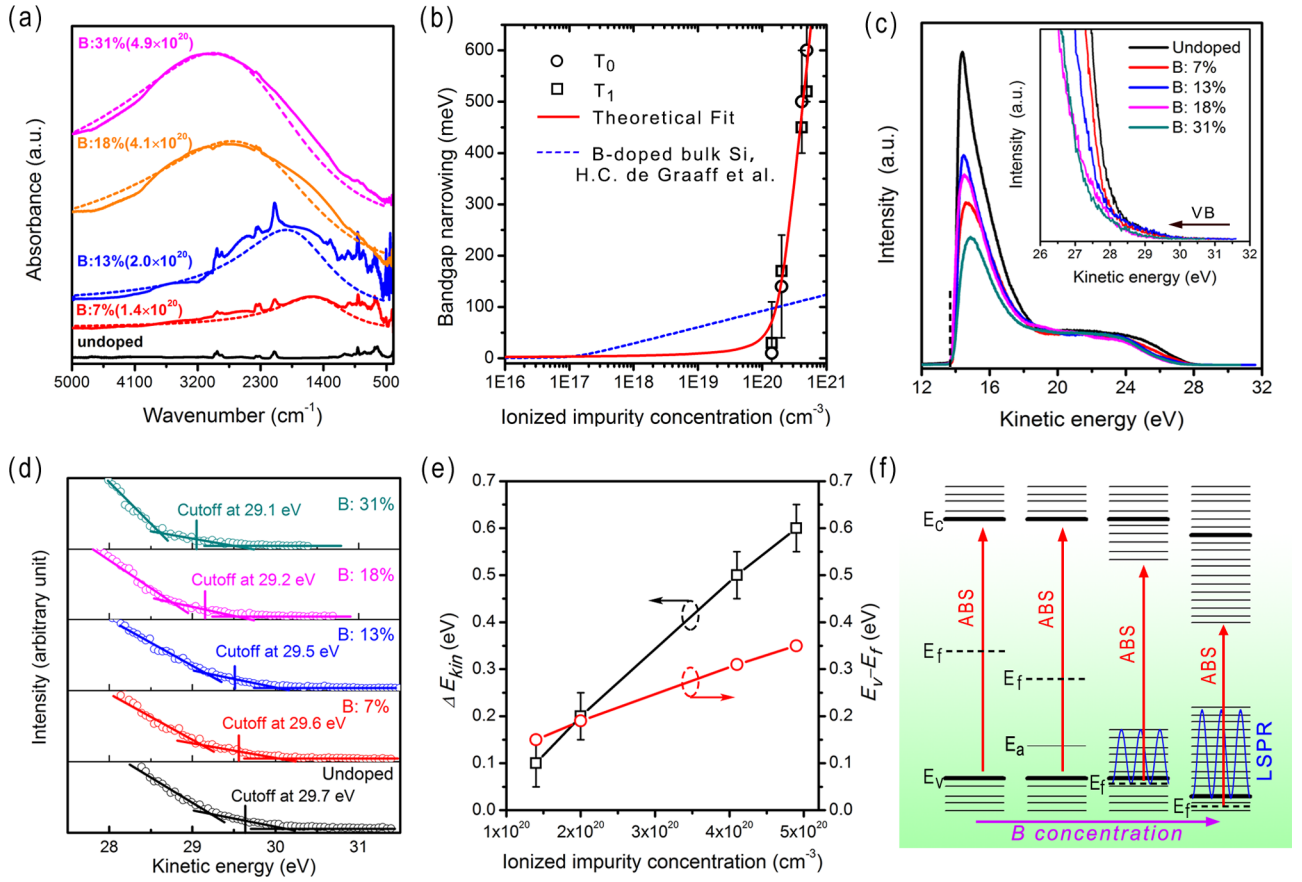

Figure 4. (a) FTIR spectra of undoped and heavily B-doped Si NCs after HF vapor etching. The dash lines show the fitting of LSPR-induced absorption for each heavily B-doped Si NCs by using the Drude model. The free carrier concentrations obtained from the fitting are also indicated in parentheses. (b) Band-gap narrowing associated with the indirect transition (T_0) and direct transition (T_1) obtained in heavily B-doped Si NCs. Graaff et al.'s results for band-gap narrowing in heavily B-doped bulk Si[55] are shown for comparison. (c) UPS spectra of undoped and heavily B-doped Si NCs. The inset shows the magnified spectra in the Si valence-band-edge region. (d) Valence-band edges of undoped and heavily B-doped Si NCs taken as the center of the slope indicated by the verticle lines. (e) Comparison of the shift of valence-band edge (ΔE_{kin}) and E_v−E_f calculated from eq 3. (f) Evolution of the Si NC band structure with the increase of the doping level of B. The B concentration increases from left to right. ABS, absorption onset; E_c, conduction-band edge; E_v, valence-band edge; E_f, Fermi energy level; E_a, impurity energy level.

core side.[44] We believe that ionized B atoms at the surface/subsurface of heavily B-doped Si NCs produce a negative potential that is strong enough to effectively retard the agglomeration of heavily B-doped Si NCs in the current work. Indeed we have measured a zeta potential of −26 mV for the heavily B-doped Si NCs in benzonitrile, approaching ±30 mV, which is usually considered to be sufficient for long-term stability. It appears that a thin oxide layer at the surface of heavily B-doped Si NCs cannot seriously screen the B-induced negative potential at the NC surface. This explains the excellent colloidal stability of heavily B-doped Si NCs during long-time storage in air.

Direct and Indirect Electronic Transitions. The excellent dispersion of heavily B-doped Si NCs in benzonitrile facilitates the study on the electronic transitions of heavily B-doped Si NCs by using optical absorption measurements. Figure 3a shows the optical absorption spectra of heavily B-doped Si NCs in benzonitrile. The optical absorption spectrum of Cl-passivated Si NCs in benzonitrile is also included for comparison. As an indirect band-gap semiconductor, bulk Si is characteristic of an indirect Γ−X transition (T_0) and a direct Γ−Γ transition (T_1) (inset of Figure 3a). As expected from the Mie theory,[45,46] a shoulder associated with the T_1 transition can be identified in each spectrum in Figure 3a. However, we do not observe a clear sign for the T_0 transition from the spectra, largely due to the weak band-edge absorption of Si.[47] The energy of the T_1 transition (E_1) can be determined by examining the derivation of an absorption spectrum, as demonstrated in Figure 3b. Specifically, Cl-passivated Si NCs show the T_1 transition at 3.58 eV, similar to that obtained by Gresback et al.[45] As the B concentration increases from ∼7% to 31%, the T_1 transition monotonically red-shifts from 3.55 eV to 3.06 eV.

To investigate whether heavy B doping also leads to the change of the T_0 transition, we employ the Tauc law to analyze the optical absorption spectra.[48] For an indirect semiconductor, the relationship between absorption cross section (σ) and the energy of the T_0 transition (E_0) is given by[49]

$$\sigma\hbar\omega \propto \omega^{-1}(\hbar\omega - E_0)^2 \quad (1)$$

where $\hbar\omega$ is the photon energy. According to eq 1, each optical absorption spectrum in Figure 3a is replotted, leading to the results shown in Figure 3c. We see that there is a soft onset, followed by an almost linear increase in each spectrum. E_0 can be extracted by fitting the linear increase of each curve in Figure 3c. For Cl-passivated Si NCs, we obtain that E_0 is 1.5 eV, consistent with the quantum confinement effect.[50] After Si NCs are heavily doped with B E_0 red-shifts. When the concentration

DOI: 10.1021/acsphotonics.5b00568
ACS Photonics 2016, 3, 415−422

of B reaches ~31%, E_0 decreases to 0.9 eV. The apparent red-shift of the absorption onset (i.e., T_0) is actually consistent with the change of Si NC color from dark yellow to black as the doping level of B increases (Figure S4 in the Supporting Information).

Band-Gap Narrowing. Figure 4a shows the FTIR spectra of undoped and heavily B-doped Si NCs. Heavy B doping leads to a broad absorption peak that blue-shifts from ~1528 cm^{-1} to 3020 cm^{-1} with the increase of B doping level. This is characteristic of the heavy-doping-induced LSPR of Si NCs.[8,9,11,29] After analyzing the LSPR-induced absorption peak of heavily B-doped Si NCs by using the Mie absorption theory with the Drude contribution,[9] we obtain that free carrier (hole) concentrations of Si NCs doped with ~7%, 13%, 18%, and 31% B are ~1.4×10^{20}, 2.0×10^{20}, 4.1×10^{20}, and 4.9×10^{20} cm^{-3}, respectively. Clearly, there is a great deal of un-ionized B atoms in Si NCs despite the current rather high free carrier concentrations. In the meantime, we should note that the high free carrier concentrations in heavily B-doped Si NCs are consistent with the aforementioned red-shifts of T_0 and T_1 (i.e., band-gap narrowing) if we assume the similarity of Si NCs to bulk Si.[51−53]

Figure 4b shows the dependence of the band-gap narrowing on the ionized impurity concentration. It is seen that the narrowing of T_1 is basically consistent with that of T_0 as the ionized impurity concentration varies. This may be because heavy B doping introduces an impurity band close to the valence band at the Γ point.[53] In the meantime, the conduction band at both the Γ and X points moves toward the band gap.[52,54] Therefore, the T_0 and T_1 transitions are nearly equally affected. It is known that in bulk Si the band-gap narrowing (ΔE_g) is given as a function of the concentration (N) of the ionized impurity:[51]

$$\Delta E_g = C_1\left\{\ln\left(\frac{N}{N_1}\right) + \sqrt{\left[\ln\left(\frac{N}{N_1}\right)\right]^2 + C_2}\right\} \quad (2)$$

where N_1 is a critical parameter, indicating the onset of the band-gap narrowing, and C_1 and C_2 are constants. Figure 4b shows the typical fit for the band-gap narrowing of heavily B-doped Si NCs by use of eq 2. The value of N_1 derived from the fitting is 1.8×10^{20} cm^{-3}. This means that the band gap of Si NCs starts decreasing when the ionized B concentration is larger than 1.8×10^{20} cm^{-3}. Such a critical value is more than 3 orders of magnitude higher than that obtained for heavily B-doped bulk Si (1.3×10^{17} cm^{-3}).[55] The quantum confinement effect may cause the energy levels of B to be deeper in the band gap for Si NCs than bulk Si.[56,57] Therefore, a much larger B concentration is needed to form an impurity band extending to the valence band and narrow the bandgap in Si NCs than in bulk Si. Moreover, C_1 increases from 6.7 for B-doped bulk Si to 270 for heavily B-doped Si NCs, indicating that the band gap shrinks more significantly in Si NCs than in bulk Si. This may be due to the fact that a number of un-ionized B atoms give rise to increased disorder in Si NCs, causing the dispersion of impurity energy levels to increase.[58,59] Therefore, the shrinking of the band gap of Si NCs is enhanced.

After heavy B doping the Fermi level (E_f) should enter the original valence band, leading to the degeneracy of the valence band.[60] The free carrier (hole) concentration (p) is related to the energy difference between the Fermi level and original valence-band edge ($E_v - E_f$) as[60]

$$p = \frac{2(2\pi m_h k_0 T)^{3/2}}{h^3}\frac{2}{\sqrt{\pi}}\int_0^\infty \frac{x^{1/2}}{1 + e^{(x-(E_v-E_f)/k_0T)}}\,dx \quad (3)$$

where m_h is the effective mass of a hole, T is temperature, h is Planck constant, and k_0 is Boltzmann constant. We work out that $E_v - E_f$ are ~0.15, 0.19, 0.31, and 0.35 eV when Si NCs are doped with ~7%, 13%, 18%, and 31% B, respectively. To examine the shift of the Fermi level into the valence band, we have carried out ultraviolet photoelectron spectroscopy (UPS) measurements for both undoped and heavily B-doped Si NCs. The results are shown in Figure 4c. The UPS spectra are obtained by using a 21.2 eV He-Ia source with an applied bias voltage of −9.8 eV to separate the secondary electron edges between a sample and the spectrometer. It is seen that the secondary electron backgrounds of all Si NCs cut off at 13.6 eV, as indicated by the dash line in Figure 4c. Therefore, we can evaluate the position of the Fermi level from the change of the valence-band edge.[61] The inset of Figure 4c shows the magnified spectra in the Si valence-band-edge region. Ideally, the valence-band edges should be infinitely abrupt. However, due to limited instrument resolution and thermal effect, they are broadened. The actual positions of the edges can be determined as the centers of the slope, as shown in Figure 4d.[62] For undoped Si NCs we obtain that the valence-band edge cuts off at 29.7 eV. The ionization energy of undoped Si NCs is thus calculated to be 5.1 eV (Figure S5a in the Supporting Information), which is 0.2 eV larger than that of bulk Si (4.9 eV).[63] This is in good agreement with the valence-band shift induced by the quantum confinement effect.[64] With the B doping level increases to 31%, the valence-band edge monotonically shifts from 29.7 eV to 29.1 eV. The shift of the valence-band edge (ΔE_{kin}) and $E_v - E_f$ obtained from eq 3 are compared in Figure 4e. It is found that ΔE_{kin} agrees with $E_v - E_f$ when the ionized impurity concentration is $<2 \times 10^{20}$ cm^{-3}. This suggests the red-shift of the valence-band edge is basically due to the move of the Fermi level into the original valence band (Figure S5b in the Supporting Information). As the ionized impurity concentration increases to $>2 \times 10^{20}$ cm^{-3}, ΔE_{kin} significantly exceeds $E_v - E_f$. For Si NCs doped with B at the highest concentration of 31%, the obtained ΔE_{kin} is 0.6 eV, which is nearly 2 times larger than $E_v - E_f$. This indicates that the original valence-band edge also moves downward in addition to the Fermi level moving into the original valence band (Figure S5c in the Supporting Information). The decrease of the original valence-band edge is possibly due to the tensile strain induced by heavy B doping.[23,65,66]

If the move of the conduction band toward the band gap was less significant than that of the Fermi level into the original valence band, the widening of the indirect/direct (optical) band gap (the increase of E_0/E_1), i.e., the so-called Burstein−Moss shift,[67] would be observed. Since we actually observe the decrease of both E_0 and E_1 after heavy B doping, the conduction band ought to significantly move toward the band gap as the Fermi level enters the original valence band, as schematically shown in Figure 4d. With the increase of the B concentration, the B-induced impurity band becomes more extended to occupy a larger part of the original band gap. In the meantime, the conduction band more significantly moves toward the band gap, while the Fermi level basically remains within the top region of the original valence band. This explains the continuous red-shift of the optical absorption with the increase of the B concentration. Because the B-induced

DOI: 10.1021/acsphotonics.5b00568
ACS Photonics 2016, 3, 415−422

impurity band is merged with the original valence band after heavy B doping, free holes above the Fermi level are largely from the B-induced impurity band. The collective oscillation of these free holes should occur under external excitation, leading to LSPR.[29]

CONCLUSION

In summary, tunable plasmonic properties and colloidal stability without the use of ligands are demonstrated for heavily B-doped Si NCs. Ionized B atoms induce a negative potential at the NC surface, which is proposed to be responsible for the colloidal stability of Si NCs in solvent. Heavily B-doped Si NC colloids are found to be stable in air for months, making them suitable for the device processing in ambient atmosphere. The effect of heavy B doping on the band structure of Si NCs has been explored by optical absorption. It is found that heavy B doping significantly decreases the energies of both the indirect and direct electronic transitions in Si NCs. This decrease could be interpreted by the move of the conduction band toward the band gap, which could be more significant than that of the Fermi level into the valence band. The plasmonic and subinterband absorption of Si NCs enabled by heavy B doping is located in the infrared regime in the current work, which should be helpful to the development of novel Si-based optoelectronic structures and devices.[68]

METHODS

Si NC Synthesis. Undoped Si NCs were synthesized by introducing SiH_4 (10% in Ar) and Ar into a nonthermal plasma chamber. The synthesis of B-doped Si NCs was realized by including B_2H_6 (0.5% in Ar) into the SiH_4/Ar nonthermal plasma. The flow rate of B_2H_6 was changed from 0.88 standard cubic centimeter per minute (sccm) to 15.2 sccm, while the flow rate of SiH_4 was kept at 31.5 sccm. The total gas flow rate was fixed at 3820 sccm, and the pressure was maintained at 360 Pa. For synthesizing Cl-passivated Si NCs, $SiCl_4$ was employed as the silicon precursor. The flow rate of $SiCl_4$, H_2, and Ar introduced into the plasma chamber was 7, 140, and 560 sccm, respectively, leading to a pressure of 400 Pa. The power for synthesizing all Si NCs was ∼200 W.

Preparation of Si NC Colloids. HF vapor etching of oxidized Si NCs was performed in a Teflon container at room temperature for 4 h. The etched NCs were placed in a vacuum for 2 h to remove the excess HF for further analysis. Undoped Si NC colloid was prepared by adding the etched undoped Si NCs into benzonitrile followed by ultrasonication for 3 min with a tip-ultrasonicator (Sonic & Materials, Inc., VCX130PB) at ∼2 W. Heavily B-doped Si NC colloids were prepared by adding the etched heavily B-doped Si NCs into benzonitrile without ultrasonication.

Characterization of Si NCs and Si NC Films. The concentrations of B for heavily doped Si NCs were determined by standard chemical titration measurements. Heavily B-doped Si NCs were reacted with solid KOH in a nickel crucible. The product was then transferred to a plastic cup containing HNO_3 to form silicic and boracic (phosphoric) acids. Excessive potassium chloride and potassium fluoride were added to the plastic cup to fully precipitate potassium fluorosilicate and potassium fluoroborate (fluorophosphate). These precipitates were then hydrolyzed in water, resulting in the formation of HF. The resulting solution was finally treated by a standard NaOH titration method, in which phenolphthalein was employed as an indicator for the end of titration. For TEM measurements, samples were prepared by drop-casting the Si NC colloid onto a copper grid coated with carbon film. Each sample was gently heated to evaporate solvent before being inserted into the microscope. TEM measurements were performed by FE-TEM 2010F with an acceleration voltage of 200 kV. Zeta potential measurements were carried out on the NC colloids by using a Zetasizer Nano-ZS (Malvern Instrument). Photoelectron spectroscopy measurements were performed by using a Kratos AXIS Ultra DLD. XPS measurements were carried out with a monochromatic Al Kα X-ray source. Samples for XPS were prepared by placing HF-etched Si NCs on carbon-tape-covered aluminum substrates. UPS measurements were carried out with a 21.2 eV He-Ia source and a −9.8 eV bias. Samples for UPS were prepared by placing the HF-etched Si NCs on ITO-coated glass substrates.

Si NC films were fabricated in air by drop-casting the Si NC colloids onto a Si substrate. A small funnel was placed over a film to slow the evaporation. SEM images were obtained by using a Hitachi S4000 field emission microscope at an acceleration voltage of 25 kV. AFM images were obtained by using a Shimadzu SPM-9600.

Optical Characterization. A UV−vis spectrometer (Shimadzu UV-2000) was used to measure the optical absorption of Si NCs. Samples for UV−vis were diluted NC colloids contained in quartz cuvettes with a path length of 10 mm. All the measurements were carried out at a resolution of 4 nm. Samples for FTIR measurements were prepared by drop-casting Si NC colloids on a thallium bromoiodide (KRS-5) substrate. Si NCs were self-assembled into films after solvent evaporation. A FTIR spectrometer (JASCO FT/IR-6100) operated in the transmission mode with a resolution of 4 cm^{-1} was used to measure all the samples.

ASSOCIATED CONTENT

Supporting Information

The Supporting Information is available free of charge on the ACS Publications website at DOI: 10.1021/acsphotonics.5b00568.

TEM results of undoped Si NCs, heavily B-doped Si NCs, and Cl-passivated Si NCs; derivative optical absorption spectra of undoped Si NCs, Cl-passivated Si NCs, and heavily B-doped Si NCs in benzonitrile; absorption spectra for the heavily B-doped Si NCs in benzonitrile after they are stored in air for 0 day, 2 weeks, and 4 months; photographs of undoped and heavily B-doped Si NC powders; schematic of photoemission spectroscopy on undoped and heavily B-doped Si NCs (PDF)

AUTHOR INFORMATION

Corresponding Authors

*E-mail: xdpi@zju.edu.cn (X. Pi).
*E-mail: tnozaki@mech.titech.ac.jp (T. Nozaki).

Notes

The authors declare no competing financial interest.

ACKNOWLEDGMENTS

This work is supported by Grant-in-Aid for Scientific Research (B) (26289045), National Basic Research Program of China (Grant No. 2013CB632101), and the NSFC for Excellent Young Researchers (Grant No. 61222404). We thank Prof.

DOI: 10.1021/acsphotonics.5b00568
ACS Photonics 2016, 3, 415−422

Hidetoshi Matsumoto, Dept. of Organic and Polymer Materials of Tokyo Institute of Technology, for providing the UV−vis measurements. The Center for Advanced Materials Analysis of Tokyo Institute of Technology is acknowledged for providing TEM, SEM, and AFM characterizations.

REFERENCES

(1) Liu, X.; Swihart, M. T. Heavily-Doped Colloidal Semiconductor and Metal Oxide Nanocrystals: An Emerging New Class of Plasmonic Nanomaterials. *Chem. Soc. Rev.* **2014**, *43*, 3908−3920.
(2) Naik, G. V.; Shalaev, V. M.; Boltasseva, A. Alternative Plasmonic Materials: Beyond Gold and Silver. *Adv. Mater.* **2013**, *25*, 3264−3294.
(3) Faucheaux, J. A.; Stanton, A. L. D.; Jain, P. K. Plasmon Resonances of Semiconductor Nanocrystals: Physical Principles and New Opportunities. *J. Phys. Chem. Lett.* **2014**, *5*, 976−985.
(4) Luther, J. M.; Jain, P. K.; Ewers, T.; Alivisatos, A. P. Localized Surface Plasmon Resonances Arising From Free Carriers in Doped Quantum Dots. *Nat. Mater.* **2011**, *10*, 361−366.
(5) Manthiram, K.; Alivisatos, A. P. Tunable Localized Surface Plasmon Resonances in Tungsten Oxide Nanocrystals. *J. Am. Chem. Soc.* **2012**, *134*, 3995−3998.
(6) Buonsanti, R.; Llordes, A.; Aloni, S.; Helms, B. A.; Milliron, D. J. Tunable Infrared Absorption and Visible Transparency of Colloidal Aluminum-Doped Zinc Oxide Nanocrystals. *Nano Lett.* **2011**, *11*, 4706−4710.
(7) Kanehara, M.; Koike, H.; Yoshinaga, T.; Teranishi, T. Indium Tin Oxide Nanoparticles with Compositionally Tunable Surface Plasmon Resonance Frequencies in the Near-IR Region. *J. Am. Chem. Soc.* **2009**, *131*, 17736−17737.
(8) Rowe, D. J.; Jeong, J. S.; Mkhoyan, K. A.; Kortshagen, U. R. Phosphorus-Doped Silicon Nanocrystals Exhibiting Mid-Infrared Localized Surface Plasmon Resonance. *Nano Lett.* **2013**, *13*, 1317−1322.
(9) Zhou, S.; Pi, X.; Ni, Z.; Ding, Y.; Jiang, Y.; Jin, C.; Delerue, C.; Yang, D.; Nozaki, T. Comparative Study on the Localized Surface Plasmon Resonance of Boron- and Phosphorus-Doped Silicon Nanocrystals. *ACS Nano* **2015**, *9*, 378−386.
(10) Schimpf, A. M.; Knowles, K. E.; Carroll, G. M.; Gamelin, D. R. Electronic Doping and Redox-Potential Tuning in Colloidal Semiconductor Nanocrystals. *Acc. Chem. Res.* **2015**, *48*, 1929−1937.
(11) Kramer, N. J.; Schramke, K. S.; Kortshagen, U. R. Plasmonic Properties of Silicon Nanocrystals Doped with Boron and Phosphorus. *Nano Lett.* **2015**, *15*, 5597−5603.
(12) Habas, S. E.; Platt, H. A. S.; van Hest, M. F. A. M.; Ginley, D. S. Low-Cost Inorganic Solar Cells: From Ink to Printed Device. *Chem. Rev.* **2010**, *110*, 6571−6594.
(13) Williams, B. A.; Mahajan, A.; Smeaton, M. A.; Holgate, C. S.; Aydil, E. S.; Francis, L. F. Formation of Copper Zinc Tin Sulfide Thin Films from Colloidal Nanocrystal Dispersions via Aerosol-Jet Printing and Compaction. *ACS Appl. Mater. Interfaces* **2015**, *7*, 11526−11535.
(14) Pi, X. D.; Zhang, L.; Yang, D. R. Enhancing the Efficiency of Multicrystalline Silicon Solar Cells by the Inkjet Printing of Silicon-Quantum-Dot Ink. *J. Phys. Chem. C* **2012**, *116*, 21240−21243.
(15) Kim, B. H.; Onses, M. S.; Lim, J. B.; Nam, S.; Oh, N.; Kim, H.; Yu, K. J.; Lee, J. W.; Kim, J. H.; Kang, S. K.; Lee, C. H.; Lee, J.; Shin, J. H.; Kim, N. H.; Leal, C.; Shim, M.; Rogers, J. A. High-Resolution Patterns of Quantum Dots Formed by Electrohydrodynamic Jet Printing for Light-Emitting Diodes. *Nano Lett.* **2015**, *15*, 969−973.
(16) Luther, J. M.; Law, M.; Song, Q.; Perkins, C. L.; Beard, M. C.; Nozik, A. J. Structural, Optical and Electrical Properties of Self-Assembled Films of PbSe Nanocrystals Treated with 1,2-ethanedithiol. *ACS Nano* **2008**, *2*, 271−280.
(17) Heath, J. R.; Shiang, J. J. Covalency in Semiconductor Quantum Dots. *Chem. Soc. Rev.* **1998**, *27*, 65−71.
(18) Murray, C. B.; Norris, D. J.; Bawendi, M. G. Synthesis and Characterization of Nearly Monodisperse CdE (E = S, Se, Te) Semiconductor Nanocrystallites. *J. Am. Chem. Soc.* **1993**, *115*, 8706−8715.
(19) Veinot, J. G. C. Synthesis, Surface Functionalization, and Properties of Freestanding Silicon Nanocrystals. *Chem. Commun.* **2006**, 4160−4168.
(20) Mangolini, L.; Kortshagen, U. Plasma-Assisted Synthesis of Silicon Nanocrystal Inks. *Adv. Mater.* **2007**, *19*, 2513−2519.
(21) Yin, Y.; Alivisatos, A. P. Colloidal Nanocrystal Synthesis and the Organic−Inorganic Interface. *Nature* **2005**, *437*, 664−670.
(22) Norris, D. J.; Efros, A. L.; Erwin, S. C. Doped Nanocrystals. *Science* **2008**, *319*, 1776−1779.
(23) Zhou, S.; Pi, X. D.; Ni, Z. Y.; Luan, Q. B.; Jiang, Y. Y.; Jin, C. H.; Nozaki, T.; Yang, D. Boron- and Phosphorus-Hyperdoped Silicon Nanocrystals. *Part. Part. Syst. Charact.* **2015**, *32*, 213−221.
(24) Erwin, S. C.; Zu, L.; Haftel, M. I.; Efros, A. L.; Kennedy, T. A.; Norris, D. J. Doping Semiconductor Nanocrystals. *Nature* **2005**, *436*, 91−94.
(25) Law, M.; Luther, J. M.; Song, O.; Hughes, B. K.; Perkins, C. L.; Nozik, A. J. Structural, Optical, and Electrical Properties of PbSe Nanocrystal Solids Treated Thermally or with Simple Amines. *J. Am. Chem. Soc.* **2008**, *130*, 5974−5985.
(26) Chen, T.; Skinner, B.; Xie, W.; Shklovskii, B. I.; Kortshagen, U. R. Carrier Transport in Films of Alkyl-Ligand-Terminated Silicon Nanocrystals. *J. Phys. Chem. C* **2014**, *118*, 19580−19588.
(27) Talapin, D. V.; Murray, C. B. PbSe Nanocrystal Solids for N- and P-Channel Thin Film Field-Effect Transistors. *Science* **2005**, *310*, 86−89.
(28) Zabet-Khosousi, A.; Dhirani, A. A. Charge Transport in Nanoparticle Assemblies. *Chem. Rev.* **2008**, *108*, 4072−4124.
(29) Pi, X. D.; Delerue, C. Tight-Binding Calculations of the Optical Response of Optimally P-Doped Si Nanocrystals: A Model for Localized Surface Plasmon Resonance. *Phys. Rev. Lett.* **2013**, *111*, 177402.
(30) Wheeler, L. M.; Neale, N. R.; Chen, T.; Kortshagen, U. R. Hypervalent Surface Interactions for Colloidal Stability and Doping of Silicon Nanocrystals. *Nat. Commun.* **2013**, *4*, 2197−2206.
(31) Zhou, S.; Ding, Y.; Pi, X.; Nozaki, T. Doped Silicon Nanocrystals from Organic Dopant Precursor by a $SiCl_4$-Based High Frequency Nonthermal Plasma. *Appl. Phys. Lett.* **2014**, *105*, 183110.
(32) Gresback, R.; Nozaki, T.; Okazaki, K. Synthesis and Oxidation of Luminescent Silicon Nanocrystals from Silicon Tetrachloride by Very High Frequency Nonthermal Plasma. *Nanotechnology* **2011**, *22*, 305605.
(33) Zou, J.; Kauzlarich, S. Functionalization of Silicon Nanoparticles via Silanization: Alkyl, Halide and Ester. *J. Cluster Sci.* **2008**, *19*, 341−355.
(34) Nozaki, T.; Sasaki, K.; Ogino, T.; Asahi, D.; Okazaki, K. Microplasma Synthesis of Tunable Photoluminescent Silicon Nanocrystals. *Nanotechnology* **2007**, *18*, 235603.
(35) Mangolini, L.; Thimsen, E.; Kortshagen, U. High-Yield Plasma Synthesis of Luminescent Silicon Nanocrystals. *Nano Lett.* **2005**, *5*, 655−659.
(36) Pi, X.; Li, Q.; Li, D.; Yang, D. Spin-Coating Silicon-Quantum-Dot Ink to Improve Solar Cell Efficiency. *Sol. Energy Mater. Sol. Cells* **2011**, *95*, 2941−2945.
(37) Pi, X. D.; Gresback, R.; Liptak, R. W.; Campbell, S. A.; Kortshagen, U. Doping Efficiency, Dopant Location, and Oxidation of Si Nanocrystals. *Appl. Phys. Lett.* **2008**, *92*, 123102.
(38) Niesar, S.; Pereira, R. N.; Stegner, A. R.; Erhard, N.; Hoeb, M.; Baumer, A.; Wiggers, H.; Brandt, M. S.; Stutzmann, M. Low-Cost Post-Growth Treatments of Crystalline Silicon Nanoparticles Improving Surface and Electronic Properties. *Adv. Funct. Mater.* **2012**, *22*, 1190−1198.
(39) Erogbogbo, F.; Liu, T.; Ramadurai, N.; Tuccarione, P.; Lai, L.; Swihart, M. T.; Prasad, P. N. Creating Ligand-Free Silicon Germanium Alloy Nanocrystal Inks. *ACS Nano* **2011**, *5*, 7950−7959.
(40) Holman, Z. C.; Kortshagen, U. R. Nanocrystal Inks without Ligands: Stable Colloids of Bare Germanium Nanocrystals. *Nano Lett.* **2011**, *11*, 2133−2136.

DOI: 10.1021/acsphotonics.5b00568
ACS Photonics 2016, 3, 415−422

(41) Pi, X. D.; Mangolini, L.; Campbell, S. A.; Kortshagen, U. Room-Temperature Atmospheric Oxidation of Si Nanocrystals after HF Etching. *Phys. Rev. B: Condens. Matter Mater. Phys.* **2007**, *75*, 085423.
(42) Sato, K.; Fukata, N.; Hirakuri, K. Doping and Characterization of Boron Atoms in Nanocrystalline Silicon Particles. *Appl. Phys. Lett.* **2009**, *94*, 161902.
(43) Tomio, K.; Masataka, H. Coordination Number of Doped Boron Atoms in Photochemically-Deposited Amorphous Silicon Studied by X-Ray Photoelectron Spectroscopy. *Jpn. J. Appl. Phys.* **1986**, *25*, L75−L77.
(44) Sugimoto, H.; Fujii, M.; Imakita, K.; Hayashi, S.; Akamatsu, K. Phosphorus and Boron Codoped Colloidal Silicon Nanocrystals with Inorganic Atomic Ligands. *J. Phys. Chem. C* **2013**, *117*, 6807−6813.
(45) Gresback, R.; Murakami, Y.; Ding, Y.; Yamada, R.; Okazaki, K.; Nozaki, T. Optical Extinction Spectra of Silicon Nanocrystals: Size Dependence upon the Lowest Direct Transition. *Langmuir* **2013**, *29*, 1802−1807.
(46) Holman, Z. C.; Kortshagen, U. R. Absolute Absorption Cross Sections of Ligand-Free Colloidal Germanium Nanocrystals. *Appl. Phys. Lett.* **2012**, *100*, 133108.
(47) Corkish, R.; Green, M. A. Band Edge Optical Absorption in Intrinsic Silicon: Assessment of the Indirect Transition and Disorder Models. *J. Appl. Phys.* **1993**, *73*, 3988−3996.
(48) Tauc, J. Optical Properties and Electronic Structure of Amorphous Ge and Si. *Mater. Res. Bull.* **1968**, *3*, 37−46.
(49) Meier, C.; Gondorf, A.; Luettjohann, S.; Lorke, A.; Wiggers, H. Silicon Nanoparticles: Absorption, Emission, and the Nature of the Electronic Bandgap. *J. Appl. Phys.* **2007**, *101*, 103112.
(50) Delerue, C.; Allan, G.; Lannoo, M. Theoretical Aspects of the Luminescence of Porous Silicon. *Phys. Rev. B: Condens. Matter Mater. Phys.* **1993**, *48*, 11024−11036.
(51) Klaassen, D. B. M.; Slotboom, J. W.; Degraaff, H. C. Unified Apparent Bandgap Narrowing in N-Type and P-Type Silicon. *Solid-State Electron.* **1992**, *35*, 125−129.
(52) Wagner, J.; del Alamo, J. A. Bandgap Narrowing in Heavily Doped Silicon: A Comparison of Optical and Electrical Data. *J. Appl. Phys.* **1988**, *63*, 425−429.
(53) Viña, L.; Cardona, M. Effect of Heavy doping on the Optical Properties and the Band Structure of Silicon. *Phys. Rev. B: Condens. Matter Mater. Phys.* **1984**, *29*, 6739−6751.
(54) Teeffelen, S. V.; Persson, C.; Eriksson, O.; Johansson, B. Doping-Induced Bandgap Narrowing in Si Rich N- and P-Type $Si_{1-x}Ge_x$. *J. Phys.: Condens. Matter* **2003**, *15*, 489.
(55) Slotboom, J. W.; Degraaff, H. C. Measurements of Bandgap Narrowing in Si Bipolar-Transistors. *Solid-State Electron.* **1976**, *19*, 857−862.
(56) Nakamura, T.; Adachi, S.; Fujii, M.; Sugimoto, H.; Miura, K.; Yamamoto, S. Size and Dopant-Concentration Dependence of Photoluminescence Properties of Ion-Implanted Phosphorus- and Boron-Codoped Si Nanocrystals. *Phys. Rev. B: Condens. Matter Mater. Phys.* **2015**, *91*, 165424.
(57) Pi, X. D.; Chen, X. B.; Yang, D. R. First-Principles Study of 2.2 nm Silicon Nanocrystals Doped with Boron. *J. Phys. Chem. C* **2011**, *115*, 9838−9843.
(58) Suergers, C.; Wenderoth, M.; Loeser, K.; Garleff, J. K.; Ulbrich, R. G.; Lukas, M.; v Loehneysen, H. Electronic Disorder of P- and B-Doped Si at the Metal-Insulator Transition Investigated by Scanning Tunnelling Microscopy and Electronic Transport. *New J. Phys.* **2013**, *15*, 055009.
(59) Blase, X.; Bustarret, E.; Chapelier, C.; Klein, T.; Marcenat, C. Superconducting Group-IV Semiconductors. *Nat. Mater.* **2009**, *8*, 375−382.
(60) Sze, S. M. *Physics of Semiconductor Devices*; John Wiley & Sons: New York, 1969; pp 151−156.
(61) Hao, P. H.; Hou, X. Y.; Zhang, F. L.; Wang, X. Energy Band Lineup at the Porous-Silicon/Silicon Heterointerface Measured by Electron Spectroscopy. *Appl. Phys. Lett.* **1994**, *64*, 3602−3604.
(62) Park, Y.; Choong, V.; Gao, Y.; Hsieh, B. R.; Tang, C. W. Work Function of Indium Tin Oxide Transparent Conductor Measured by Photoelectron Spectroscopy. *Appl. Phys. Lett.* **1996**, *68*, 2699−2701.
(63) Melnikov, D. V.; Chelikowsky, J. R. Electron Affinities and Ionization Energies in Si and Ge Nanocrystals. *Phys. Rev. B: Condens. Matter Mater. Phys.* **2004**, *69*, 113305.
(64) Van Buuren, T.; Dinh, L. N.; Chase, L. L.; Siekhaus, W. J.; Terminello, L. J. Changes in the Electronic Properties of Si Nanocrystals as a Function of Particle Size. *Phys. Rev. Lett.* **1998**, *80*, 3803−3806.
(65) Kůsová, K.; Hapala, P.; Valenta, J.; Jelínek, P.; Cibulka, O.; Ondič, L.; Pelant, I. Direct Bandgap Silicon: Tensile-Strained Silicon Nanocrystals. *Adv. Mater. Interfaces* **2014**, *1*, 1300042.
(66) Hong, K.-H.; Kim, J.; Lee, S.-H.; Shin, J. K. Strain-Driven Electronic Band Structure Modulation of Si Nanowires. *Nano Lett.* **2008**, *8*, 1335−1340.
(67) Kamat, P. V.; Dimitrijevic, N. M.; Nozik, A. J. Dynamic Burstein-Moss Shift in Semiconductor Colloids. *J. Phys. Chem.* **1989**, *93*, 2873−2875.
(68) Rogalski, A. Infrared Detectors: Status and Trends. *Prog. Quantum Electron.* **2003**, *27*, 59−210.

DOI: 10.1021/acsphotonics.5b00568
ACS Photonics 2016, 3, 415−422